The Aeronautical Journal (2025), **129**, pp. 63–83
doi:10.1017/aer.2024.108

ROYAL AERONAUTICAL SOCIETY

RESEARCH ARTICLE

Isolating influences of varying pitch from the effects of non-zero compound angles on effusion cooling

Y. Pyo[1], J. Son[1], P. Richer[2], B. Jodoin[2], M. Broumand[3], S. Yun[3] and Z. Hong[1]

[1]University of Ottawa and National Research Council Canada, Ottawa, ON, Canada
[2]Department of Mechanical Engineering, University of Ottawa, Ottawa, ON, Canada
[3]National Research Council Canada, Aerospace Research Centre, Ottawa, ON, Canada
Corresponding author: Z. Hong; Email: zekai.hong@nrc-cnrc.gc.ca

Received: 27 October 2023; **Revised:** 8 August 2024; **Accepted:** 20 September 2024

Keywords: gas turbine; film cooling; effusion cooling; AFE (adiabatic film cooling effectiveness); PSP (pressure sensitive paint); compound angle; pitch

Abstract

Effusion cooling is the state-of-the-art cooling technology for gas turbine hot-gas path components. Typically, effusion cooling holes across the entire combustor liner are aligned with the combustor axis, rendering a nominal zero compound angle between highly directional miniature effusion cooling jets and the main flow direction. The pitch of effusion cooling holes is optimised accordingly. However, the swirling main flow results in a non-zero compound angle and an effectively different pitch from the design. The directional effect of effusion cooling as a result of swirling main flow on the adiabatic film cooling effectiveness (AFE) is a combined effect of a non-zero compound angle and a varied pitch. The current experimental study aims to investigate the isolated effects of compound angle on AFE by excluding the influences of varying pitch. With an improved understanding of the sole effects of non-zero compound angles on AFE, the roles that a varied pitch plays in modifying AFE are further discussed to guide future effusion cooling designs under swirling main flow conditions. Binary pressure sensitive paint (PSP) was used to determine AFE experimentally.

Nomenclature

AFE	adiabatic film cooling effectiveness
BR	blowing ratio
PSP	pressure sensitive paint
C	polynomial constants
d	cooling hole diameter
I	luminescent intensity
r	light intensity ratio
p	air pressure
S	Henry's law coefficient
K	Stern-Volmer constant
x	mole fraction of oxygen in air
T	temperature
U	velocity
X	concentration

This paper is a version of a presentation given at the ISABE Conference held in 2024.

https://doi.org/10.1017/aer.2024.108 Published online by Cambridge University Press

Symbols

α	inclination angle
β	compound angle
η	film cooling effectiveness

1.0 Introduction

One of the most effective approaches for improving gas turbine efficiency is to reduce the use of cooling air, as the cooling air for hot gas path components has to be compressed to the highest pressure point of the entire engine. However, the developments of more efficient gas turbine engines are typically associated with higher combustion temperatures, which in turn requires more cooling air if cooling technology remains the same, in addition to the use of advanced high-temperature materials. Furthermore, rising pressure ratios in modern gas turbine engines make the cooling of hot gas path components more challenging because the compressor air is discharged at higher temperatures, making it a less effective coolant for combustor liners and first-stage nozzles.

Inadequate cooling available for combustor liners leads to reduced combustor life expectancies and premature engine failures, as reported in the literature [1]. To reduce the metal temperature of combustor liners and to improve the longevity of hot gas path components, previous effusion cooling studies have been focusing on the shape of effusion cooling holes and the pitch of effusion cooling holes [1–4]. In addition, new ceramic materials are being developed as thermal barrier coatings for improved cooling performance [3, 4].

Multi-hole effusion cooling provides thermal protection to combustor liners by forcing air at a higher pressure through a series of pinholes, absorbing heat from the liner while forming a protective fluid film layer to insulate heat on the exposed surface [5]. The portion of air that acts as coolant is emanated from the inner surface of the liner through discrete effusion cooling holes as three-dimensional jet columns [6]. The effusion cooling does not affect the location where the coolant is injected, but rather downstream of the cooling holes [6]. Thus, the effusion cooling holes are typically designed to be in the co-linear direction with the hot main flow.

It is well established that the effusion cooling efficiency is highly dependent on the pattern and diameter of the effusion cooling holes, which govern the formation of protective films over the combustor liner. While studies on the pattern or the shape of effusion cooling holes [4–7] and coolant blowing ratios [8–10] are continuously being conducted. The directional effects of effusion cooling on adiabatic film cooling effectiveness (AFE, or η_{ad}) due to swirling main flow have not received through examinations in past studies. An earlier study [11] suggests that, for cylindrical effusion holes, maximum film effectiveness is similar for the 90° compound angle holes to that for the 0° holes and occurred at a similar momentum flux ratio. Improved film effectiveness for the 90° compound angle holes was observed for very high blowing ratios. However, a recent study [12] suggest significant directional effects of effusion cooling. It is critical to understand the directional effects of effusion cooling under realistic gas turbine combustor conditions for two reasons: 1) the effusion cooling miniature jets are highly directional while the main combustion flow inside gas turbine combustors swirls for flame stabilisation; and 2) current effusion designs predominantly have the effusion cooling holes aligned with the combustor axis. The swirling main flow induces an angular difference between effusion cooling jets and the swirling main flow. Here compound angle (β) is defined as the angular difference between the main flow and the coolant jets as shown in Fig. 1.

The swirling main flow not only induces a non-zero compound angle for effusion cooling, it also alters the effective pitch of effusion cooling holes. Fig. 2 illustrates the definition of pitch for an effusion cooling configuration. In the example effusion cooling configuration shown in the figure, the effusion cooling holes are staggered with prescribed spanwise separation between effusion hole columns (δ_x) and streamwise separation between effusion hole rows (δ_y). However, the design pitch is only valid under the condition that the main flow is strictly co-linear with effusion cooling jets, as indicated by the red arrow

https://doi.org/10.1017/aer.2024.108 Published online by Cambridge University Press

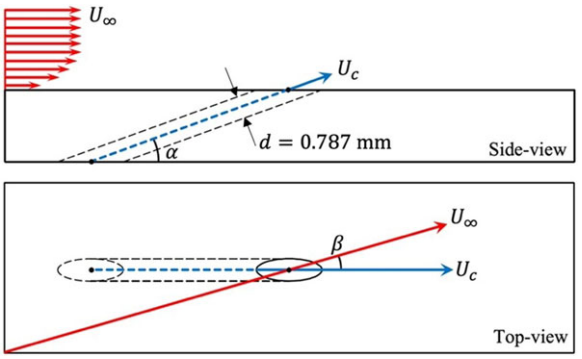

Figure 1. *Diagram of a sample effusion cooling hole with the hole diameter (d), compound angle (β) and inclination angle (α) denoted.*

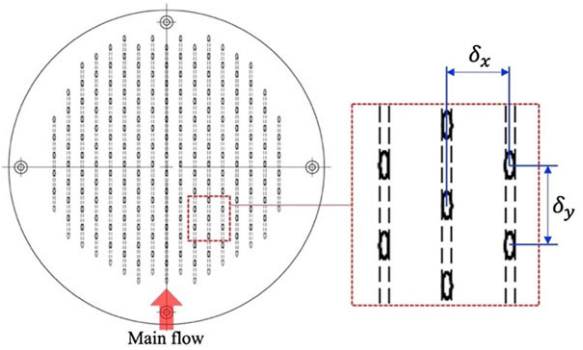

Figure 2. *Spanwise (δ_x) and streamwise (δ_y) pitches are denoted for an example effusion cooling configuration. The effusion cooling holes are staggered in this example.*

in the figure. Under swirling main flow conditions, the effective pitch is varied. To see this point, an extreme case can be considered: the main flow is introduced at 90° to the direct of effusion cooling jet from left to right. In this extreme case, the effective pitch has been altered such that the streamwise and spanwise pitches swapped. In fact, when a swirling main flow induces any non-zero angle between effusion cooling jets and the main flow, the pitch is effectively altered.

When the swirling main flow sweeps on the surface of an effusion cooling plate, both compound angle and effective pitch are altered concurrently. A recent study from this group [12] studied the two combined effects on AFE from swirling main flow as it is most relevant to practical engine operations. However, it is not clear how a non-zero compound angle and a varied pitch contribute separately to the combined directional effects of effusion cooling. The goal of this study is to separate the direction effects on AFE from a non-zero compound angle and from a varied pitch. The approach of this study is to exclude the effects of a varied pitch from the sole effects of non-zero compound angles by fixing the pitch while varying only the compound angle in the experiments. Once the isolated effects of non-zero compound angles are determined, the effects of varying effective pitch will be evaluated to guide future effusion cooling designs under swirling main flow conditions.

2.0 Methodology

Pressure sensitive paint (PSP) is a powerful experimental tool for aerodynamic and heat/mass transfer studies [13, 14], which was also adopted in previous studies for understanding effusion cooling [15–18].

https://doi.org/10.1017/aer.2024.108 Published online by Cambridge University Press

PSP was formulated by embedding oxygen-sensitive molecules in a polymer binder permeable to oxygen, enabling the inference of localised oxygen partial pressures on the paint surfaces. Upon excitation of a UV light source, the oxygen-sensitive molecules respond with varying fluorescence intensities depending on the oxygen partial pressure [19]. In the current study, nitrogen gas of 99.99% purity was used as the coolant proxy as it has effectively zero oxygen content. If an effusion cooling design is effective in producing a cooling film on the surface of a test article, the main air flow is shielded away or greatly diluted near the effusion cooling surface. Oxygen partial pressures on the surface of a test coupon as revealed by PSP fluorescence intensities can be directly correlated to adiabatic film cooling effectiveness (AFE). The fluorescence intensity and oxygen concentration can be expressed by the Stern-Volmer equation as

$$\frac{I_{max}(T)}{I(T)} = 1 + K(T) \cdot S(T, p) \cdot x \cdot p \tag{1}$$

where I is the measured PSP fluorescence intensity, I_{max} is the maximum fluorescence intensity in the absence of oxygen, K is the Stern-Volmer constant depending on temperature, S is Henry's law coefficient that is a function both of temperature and pressure, x is the mole fraction of oxygen in the gas immediately adjacent to the paint and p is the air pressure at the measurement surface. A second-order polynomial equation is adopted for calibrating PSP fluorescence intensities as following:

$$\frac{p}{p_{ref}} = C_1(T)\left(\frac{I_{ref}}{I}\right)^2 + C_2(T)\left(\frac{I_{ref}}{I}\right) + C_3(T) \tag{2}$$

where

$$\frac{I}{I_{ref}} = \frac{I_{raw} - I_{dark}}{I_{ref,\ raw} - I_{dark}} \tag{3}$$

and the subscript *ref* indicates the standard air condition as the reference point, and I_{ref} is the corrected PSP fluorescence intensity when the paint is surrounded by the standard air. On the other hand, the subscript *dark* denotes the camera reading without UV excitation, which may include some background light. In Equation (2), very weak temperature dependency of C_1, C_2, and C_3 is ignored and the polynomial coefficients are treated as constants. Equation (3) is for correcting background light leak, where the raw PSP fluorescence intensity I_{raw} is discounted by the recorded camera reading without UV excitation I_{dark} to get corrected PSP fluorescence intensity I.

However, the accuracy of local oxygen partial pressures referred from PSP fluorescence intensities can be affected by other factors, such as fluctuations in excitation illumination intensities and drifts in ambient temperature during calibration and data collection processes. In addition, errors can also arise from temperature variations on the PSP surface due to the fact that main air (ambient air) could be at a different temperature than that of coolant proxy (nitrogen), which was discharged from compressed gas bottles. To minimise uncertainties in oxygen partial pressure determinations from PSP fluorescence intensities due to the aforementioned variations, a binary PSP was used in this study. Unlike single-component PSP, the binary PSP includes a reference molecule component that enables correction for errors in PSP temperature. Fluorescence intensities can be acquired from both the oxygen-sensitive and reference molecule components allowing the errors induced by variations in PSP temperature and UV excitation illumination intensities to be compensated [18, 19]. Figure 3 shows the spectra of UV excitation illumination near 400 nm together with the resulting binary PSP fluorescence peaks near 650 nm as the pressure-sensitive signal and 560 nm as the reference signal.

The two fluorescence peaks exhibit very similar sensitivities to PSP temperature. By taking the ratio of the pressure-sensitive portion of fluorescence to the reference portion, the errors induced by variations in PSP temperature and fluctuations in UV excitation illumination intensities can be compensated. According to McLean [20], due to the imperfect mixing of two luminophores, a simple ratio of the intensities of two fluorescence peaks are insufficient to fully account for luminophore inhomogeneity. Liu et al. [21] proposed to normalise ratios of fluorescence intensities by the ratio of fluorescence intensities at the reference condition (i.e., the standard ambient air condition). The normalised ratio of fluorescence

https://doi.org/10.1017/aer.2024.108 Published online by Cambridge University Press

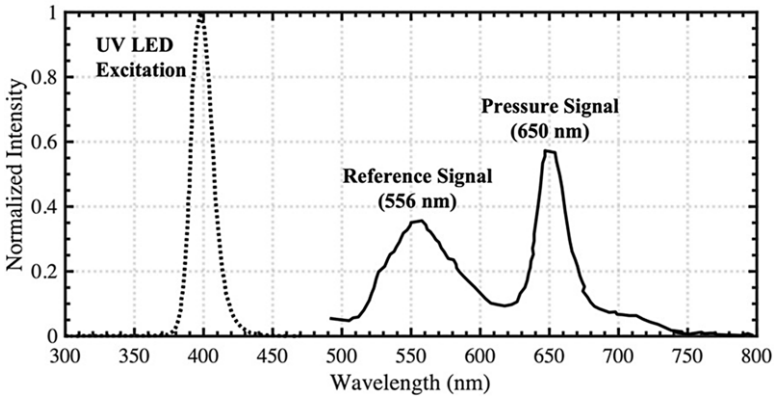

Figure 3. *Spectra of UV excitation illumination together with the resulting fluorescence peaks near 650 nm as the pressure-sensitive signal and 560 nm as the reference signal for BinaryFIB PSP from Innovative Scientific Solutions Inc. The plot is reproduced from [19].*

intensities corrects for non-homogeneous luminophore concentrations and variations in paint thickness as

$$\frac{r}{r_{ref}} = \frac{(I - I_{dark})_{PT}/(I - I_{dark})_T}{\left(I_{ref} - I_{dark}\right)_{PT}/\left(I_{ref} - I_{dark}\right)_T} \tag{4}$$

where r/r_{ref}, the normalised ratio of fluorescence intensities, replaces I/I_{ref}, normalised pressure signal fluorescence intensity introduced in Equation 2. The subscript PT indicates the pressure signal fluorescence peak near 650 nm that is both pressure and temperature dependent, while the subscript T represents the reference fluorescence peak near 560 nm that is temperature dependent only.

Adapting Equation 2 for the normalised ratio of fluorescence intensities, a second order polynomial expression is used for calibrating and determining local oxygen partial pressures on binary PSP surfaces as follows:

$$\frac{p_{O_2}}{p_{O_2,ref}} = C_1(T)\left(\frac{r_{ref}}{r}\right)^2 + C_2(T)\left(\frac{r_{ref}}{r}\right) + C_3(T) \tag{5}$$

Nitrogen is used as the coolant proxy, and ambient air is used as the main flow in this study. Since the coolant proxy is free of molecular oxygen, the local oxygen partial pressures that are determined by binary PSP using Equation 5 can be used to directly infer AFE by adopting heat/mass transfer analogy. The successful adoption of heat/mass transfer analogy requires a turbulent flow field, which is defined as having a turbulent Lewis number close to unity [22]. Due to high Reynolds numbers that are typical to gas turbine combustors (256,000 in this study), the heat/mass transfer analogy is valid over the surface of gas turbine combustor liners [23]. By accepting the heat/mass transfer analogy, AFE (η_{ad}) can be further calculated using the oxygen partial pressures determined from the normalised ratio of binary PSP fluorescence intensities using the following equation:

$$\eta_{ad} = \frac{T_g - T_{aw}}{T_g - T_c} \approx \frac{X_{O_2,g} - X_{O_2,aw}}{X_{O_2,g} - X_{O_2,c}} \tag{6}$$

where T represents temperature and X denotes mole fraction of molecular oxygen, respectively. In addition, the subscripts g, aw, and c denote main air flow, adiabatic wall and coolant, respectively.

https://doi.org/10.1017/aer.2024.108 Published online by Cambridge University Press

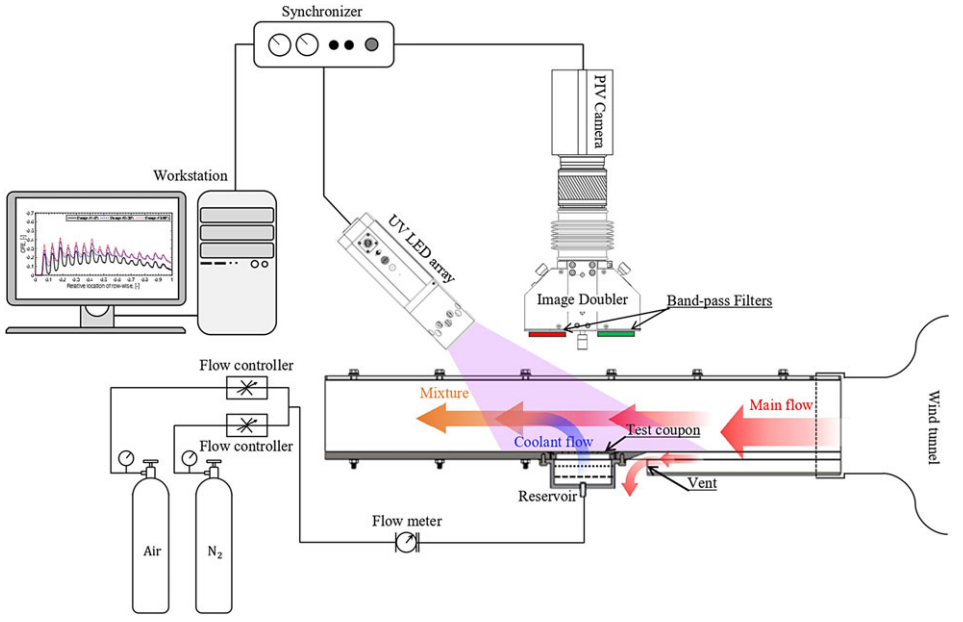

Figure 4. *Schematic of the experimental setup and a sectional view of the test section.*

3.0 Experimental setup

A lab-scale cooling test rig shown in Fig. 4 was used to evaluate the effectiveness of the current effusion cooling designs for combustor liners. The present study used a low-speed wind tunnel to accelerate ambient air as the main flow to 33 m/s in order to simulate the flow speed in a typical gas turbine combustor. In the wind tunnel, the Reynolds number and the turbulence intensity are approximately 256,000 and 3%, respectively. The wind tunnel has been described in a previous publication [24]. The wind-tunnel was driven by a 30 kW AC motor that is capable of a maximum mass flow rate of 2.5 kg/s at a pressure rise of 5 kPa.

A transparent polycarbonate top panel covers the test section. After the wind tunnel transition piece that connects the round wind tunnel outlet to the square test section, a pitot tube is located at the centre of the test section and at a distance of 228 mm from the inlet of the test section. A reservoir that has been modified by a perforated plate is used for supplying coolant proxy uniformly to all effusion cooling holes in the test coupon. The reservoir has an inner diameter of 101 mm and an internal height of 44 mm. The centre of the reservoir is located 406 mm from the inlet of the test section. Effusion cooling test coupons are installed at the bottom of the test section directly above the reservoir with the inner surface flush with the bottom of the test section.

In consistent with a previous study [16], a single round effusion cooling test coupon was designed and fabricated using stereolithography (SLA) 3D printing. The shrinkage of effusion cooling holes from 3D printing was evaluated and was compensated by post-machining to ensure effusion holes are of exact dimensions as in the previous study. The inclination angle (α) of the effusion holes is 20 degree and the diameter of effusion pinholes (d) is 0.787 mm, as illustrated in Fig. 1. The test coupon has staggered effusion cooling holes, with spanwise and streamwise separations between adjacent effusion holes 7 and 9 times of the effusion hole diameter ($\delta_x = 7d$ and $\delta_y = 9d$), as illustrated in Fig. 2.

In the previous study, a conventionally machined aluminum test coupon was installed in the test rig shown in Fig. 4 for studying the directional effects of effusion cooling. The circular test coupon was rotated so that the main flow could be at an angle with the effusion cooling jets. The arrangement mimics the realistic effusion cooling scenario in a gas turbine combustor as the swirling main flow is common

https://doi.org/10.1017/aer.2024.108 Published online by Cambridge University Press

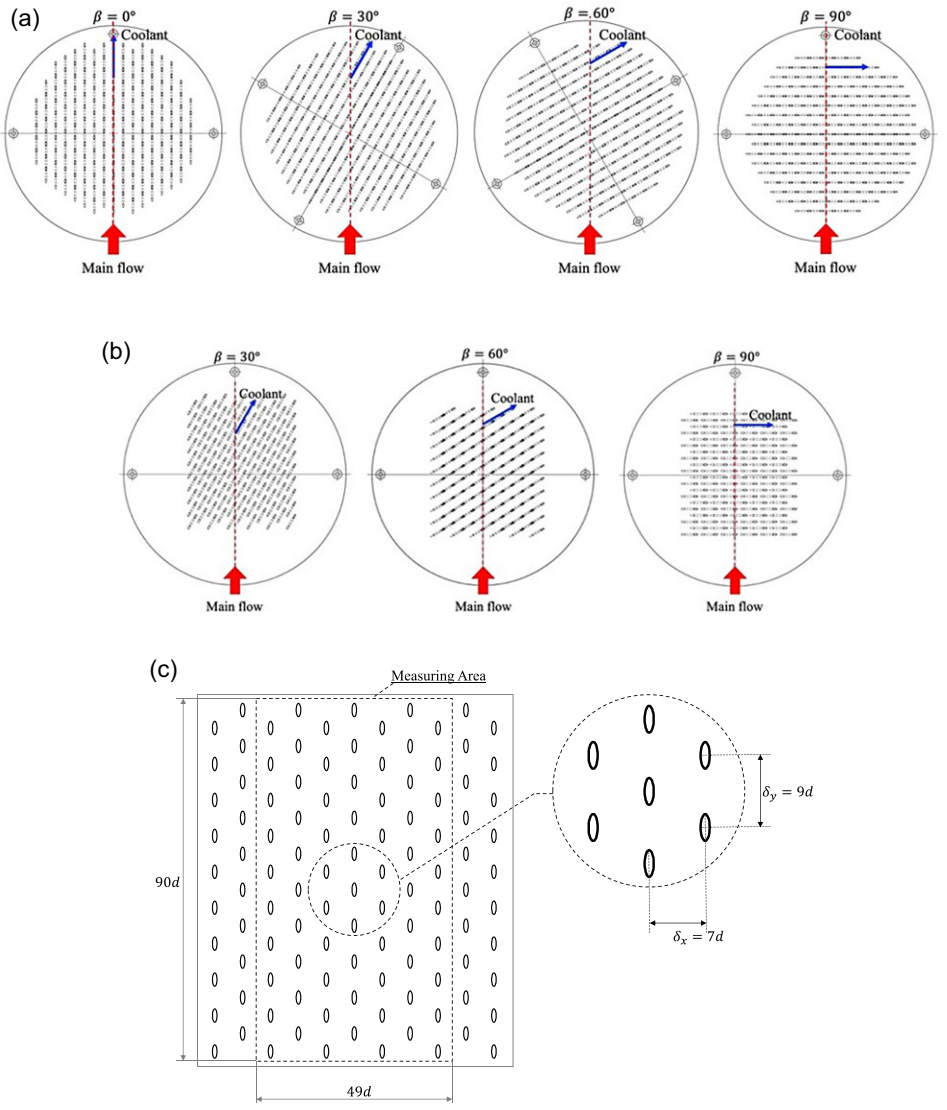

Figure 5. *Effusion cooling test configurations: (a) an identical test coupon rotated at four discrete angles relative to the main flow direction at 0°, 30°, 60°, and 90°; the co-linear installation ($\beta = 0°$, first from left) is the baseline case for all other configurations, and (b) three additional test coupons that have three discrete compound angles ($\beta = 30°,\ 60°,$ and $90°$) while maintaining a fixed pitch as the baseline case ($\delta_x = 7d$ and $\delta_y = 9d$) as shown in panel (c).*

for flame stabilisation. To verify that previous results can be reliably reproduced by an SLA 3D printed test coupon, four test configurations shown in Fig. 5(a) were first evaluated. The four test configurations shared the same test coupon. By installing the test coupon at discrete rotations, four angles, 0°, 30°, 60° and 90°, between the effusion cooling jets and the main flow were achieved. The co-linear effusion cooling configuration ($\beta = 0°$) was taken as the baseline case for comparisons throughout this study. It becomes obvious from the figure that a swirling main flow does not only induce a non-zero compound angle between effusion cooling jets and the main flow, it also alters the pitch of effusion cooling holes

https://doi.org/10.1017/aer.2024.108 Published online by Cambridge University Press

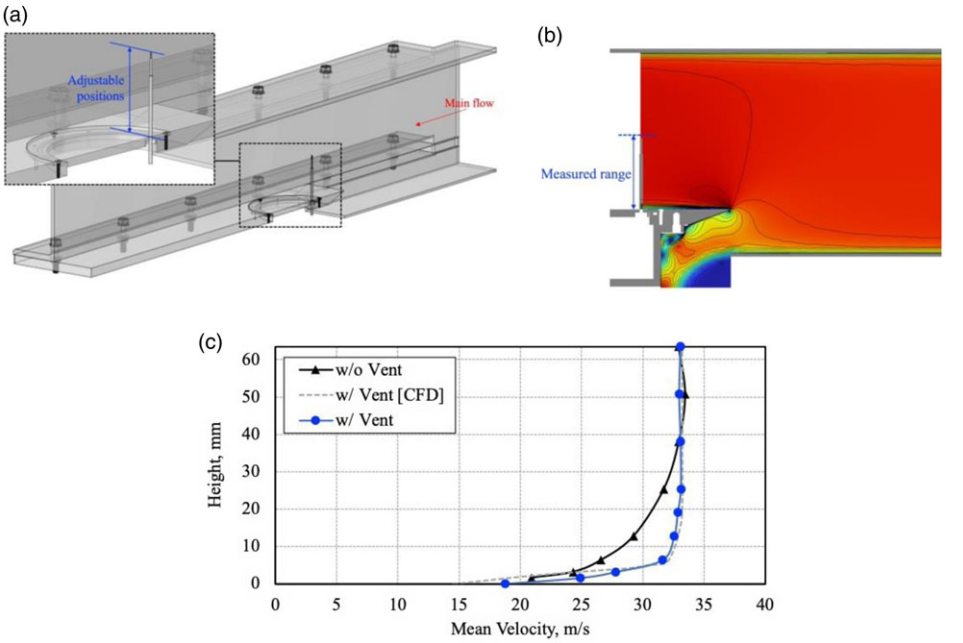

Figure 6. *(a) Cut-away view of the CAD model of the test section; the schematic details the vent for controlling boundary layer thickness on the test coupon and the installation of the hot-wire anemometer in the centre of the test section. (b) Cross-sectional view of the velocity contour near the vent for controlling boundary layer thickness from a RANS simulation. (c) Comparison of boundary layer thickness with and without the vent; results from CFD simulations are also included for comparison.*

in effect. The change in effusion cooling AFE induced by a swirling main flow is a combined effect of varied compound angles and altered pitches.

As discussed in the Introduction section, the goal of the current work is to understand the isolated effects of non-zero compound angles on effusion cooling AFE by excluding the influences of varying pitch. Also taking the co-linear effusion cooling design (first configuration from left in Fig. 5(a)) as the baseline case, new effusion cooling test coupons were designed, featuring identical effusion cooling hole pitch while the compound angle is varied as the only parameter. Besides the single test coupon shown in Fig. 5(a), three additional test coupons shown in Fig. 5(b) were fabricated with SLA 3D printing. Altogether, the comparisons can be made among four effusion cooling configurations of identical pitch and of four compound angles at 0°, 30°, 60° and 90°. It should be pointed out that for all test configurations shown in Fig. 5, only the area near the centreline is chosen for comparisons. By excluding areas on both left and right edges of the test coupon, we hope to minimise the uncertainties arise from cooling film developments in the horizontal direction.

A vent with adjustable height was designed and placed near the leading edge of the test coupons for boundary layer thickness control; the construction of the vent is shown in Fig. 6(a). CFD calculations were performed for designing the vent so that only clean stream is permitted in the test section, as shown in Fig. 6(b). The boundary layer thickness on the test coupon was measured using a hot-wire anemometer located at the leading edge of the test coupon longitudinally and in the middle of the test section horizontally, as shown in Fig. 6. In this case, the hot-wire anemometer can be adjusted to cover a height of 63.5 mm from the bottom of the test section. The momentum boundary layer thickness can be inferred from the measured velocity profile, as illustrated in Fig. 6(c).

https://doi.org/10.1017/aer.2024.108 Published online by Cambridge University Press

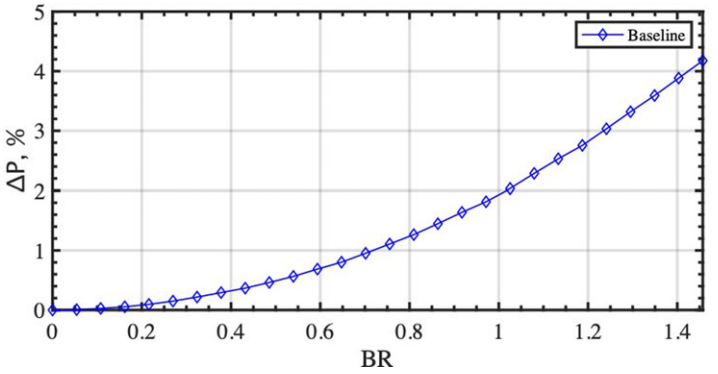

Figure 7. *The percentage pressure drop across effusion cooling test coupons were maintained as a fixed function of BR for all test configurations.*

Percentage pressure drop ΔP across effusion cooling coupons is determined by taking static pressures in the coolant reservoir and in the test section, where the static pressure in the test section is taken from the pitot tube. At blowing ratios of 0.6, 1, and 1.4, the percentage pressure drops are 0.8%, 1.8% and 3.8% respectively. Blowing ratio (BR) is an important parameter for quantifying effusion cooling and is defined by Equation 7 below. Reynolds number inside the effusion cooling holes is 1067, 1778 and 2490 at the blowing ratios of 0.6, 1 and 1.4, respectively. Blowing ratio essentially is the momentum ratio between the coolant gas and the main flow.

$$BR = \frac{\rho_c U_c}{\rho_\infty U_\infty} \tag{7}$$

where ρ_c, ρ_∞ are the densities of coolant and main flow; whereas U_c and U_∞ are the velocities of effusion cooling jets and main flow air, respectively [12]. Figure 7 shows percentage pressure drops measured as a function of BR. The wind tunnel circulates ambient air while the room temperature in the lab was maintained at 293 K.

To calibrate binary PSP specifically for our experimental setup and each effusion cooling configuration, known mixtures of neat N_2 and compressed air were used as calibration gases. Both neat N_2 and compressed air streams were regulated and metered individually and subsequently mixed in a long line. Six calibration points were taken with the volumetric fractions of compressed air at 0%, 20%, 40%, 60%, 80% and 100% with the balance gas being neat N_2. During the calibration process, the wind tunnel was turned off and the test section was isolated from the rest of the wind tunnel. The effusion cooling test coupon installed in the test section was surrounded by a calibration shrouder shown in Fig. 8(a) and was purged with calibration gases from the reservoir while maintaining the pressure in the test section at atmospheric pressure. The binary PSP on test coupon surfaces was exposed to known oxygen partial pressures while pixel-wise calibrations were being performed to get correlations between PSP fluorescence intensities and oxygen partial pressures. Once a calibration was completed for each effusion cooling configuration, the calibration shrouder was removed from the test section and the test section was reconnected back to the rest of the wind tunnel. Only N_2 was then supplied to the reservoir as the coolant proxy to visualise cooling films with the help of PSP on the surface of the effusion cooling test coupon.

In the present study, as discussed in the previous section, a binary PSP from ISSI named as BinaryFIB PSP [19] was used, which has a UV excitation peak between 380 and 520 nm and two emission peaks: 1) the pressure signal that is sensitive to oxygen partial pressure near 650 nm and 2) the reference signal near 556 nm that's insensitive to oxygen partial pressure but of almost identical temperature responses as the pressure signal. A LED light source also from ISSI (LM2X-DM) was adopted to provide UV excitation for the binary PSP near 400 nm. To acquire both PSP fluorescence signals (both pressure signal

https://doi.org/10.1017/aer.2024.108 Published online by Cambridge University Press

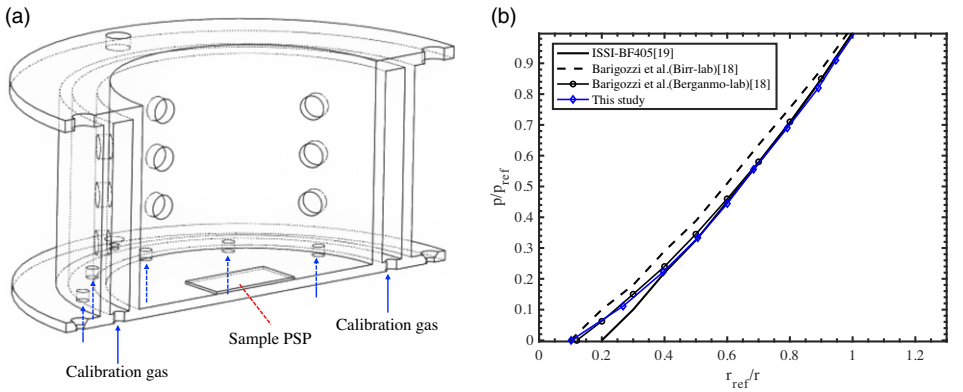

Figure 8. *(a) Schematic of the calibration shrouder being placed in the test section for isolating the effusion test coupon from the rest of the wind tunnel in the current study and (b) comparisons of calibration curves. The x-axis is the inverse of normalised ratios of fluorescence intensities as defined by Equation 4 while the y-axis is the oxygen partial pressure normalised by standard air.*

and reference signal), a LaVision ImagerProX 2M camera equipped with a LaVison Image Doubler was used. Two PSP fluorescence intensity images were filtered with bandpass filters: the first being a 650 nm centre wavelength of 20 nm FWHM (full-width at half-maximum) and the second a 560 nm centre wavelength of 10 nm FWHM. The filtered PSP fluorescence images were then combined together side-by-side by the image doubler; the combined image was subsequently acquired by the LaVision camera.

4.0 Results

4.1 PSP calibration

Figure 8(b) shows the comparisons of calibration curve of binary PSP from this study with calibration data published in the literature [18, 19]. Using the calibration curve, oxygen partial pressure as normalised by a standard air can be determined pixel-wise from normalized ratio of luminescent intensities. There are small variations among calibration curves for each pixel on the active area of the effusion cooling test coupon; the curve shown in Fig. 8(b) is the average calibration curve for all pixels of the active measurement area. The good comparisons with calibration curves published in the literature indicates the validity of the calibration procedures of the current study.

4.2 Combined effects of compound angle and varying pitch

Figure 9 presents 2D AFE (η_{ad}) maps simulating the baseline effusion cooling design being subject to various swirling main flow conditions, rendering four discrete compound angles between effusion cooling jets and mainstream, at 0°, 30°, 60° and 90°, with the effusion cooling configuration illustrated in Fig. 5. Each effusion cooling configuration was tested at three typical BR, at 0.6, 1.0 and 1.4, respectively. In these 2D AFE maps, as illustrated by the color bar of the figure, red color indicates poor quality of cooling film while blue suggests well-formed cooling film.

The directional effects present in Fig. 9 are the results of changing compound angle and effusion cooling hole pitch simultaneously. Although physically the separations between cooling hole rows and columns are maintained, however, in the direction of main flow, the pitch is altered substantially. For example, the design pitch, as is in the co-linear case, is stagged cooling hole with spanwise and streamwise separations between adjacent effusion holes 7 and 9 times of the effusion hole diameter, respectively

https://doi.org/10.1017/aer.2024.108 Published online by Cambridge University Press

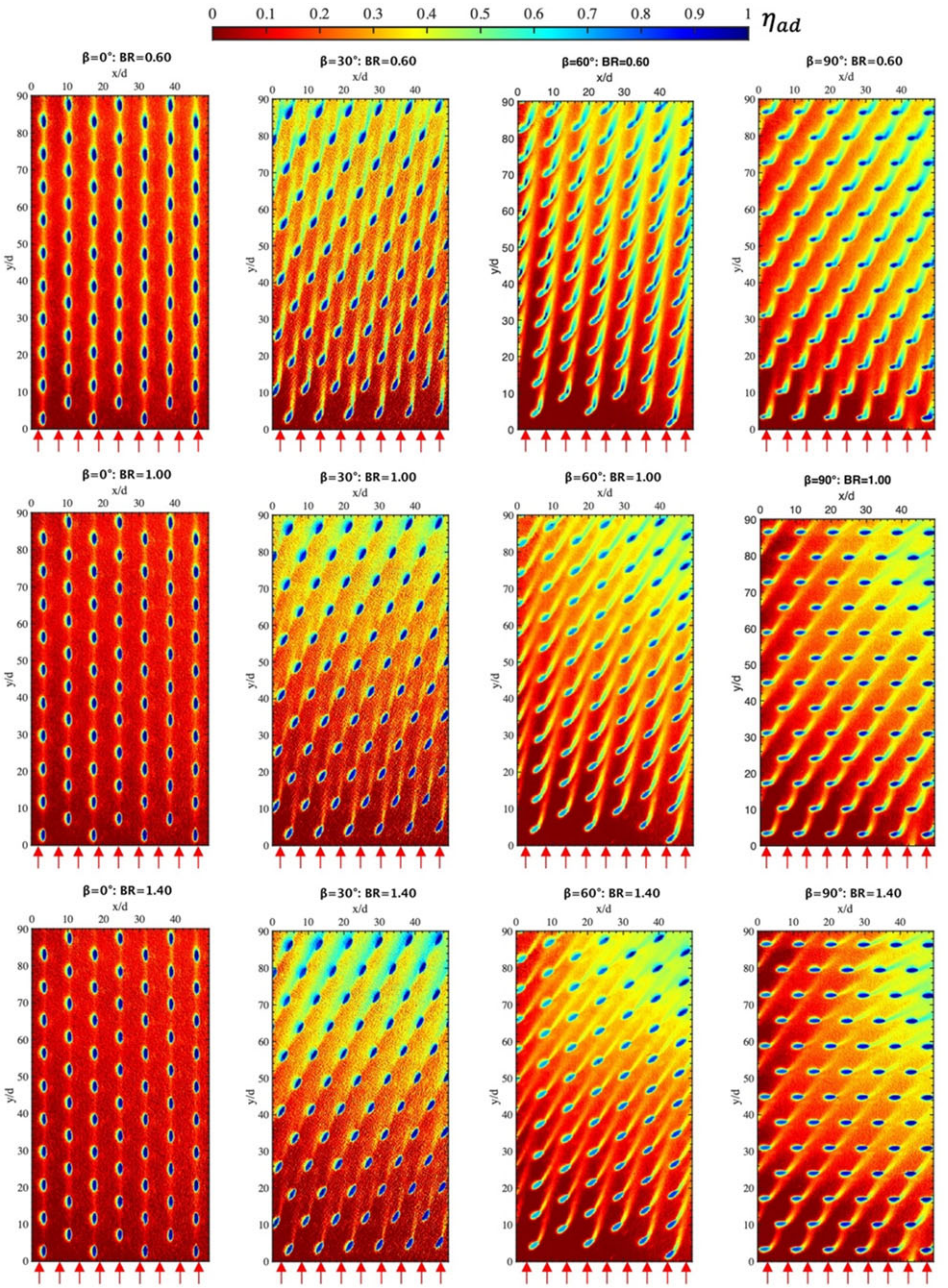

Figure 9. *Comparisons of 2D AFE distributions as the baseline effusion cooling test coupon is installed at four discrete rotation angles relative to the main flow direction (0°, 30°, 60° and 90°). The comparisons illustrate combined effects of varying compound angle and pitch on AFE that are realistic to engine combustors that are subject to swirling main flows. Red arrows indicate the main flow direction.*

($\delta_x = 7$d and $\delta_y = 9$d). However, when the effusion cooling coupon is rotated 90 degrees, the effective pitch, although still stagged, becomes $\delta_y = 7$d and $\delta_x = 9$d, as can be seen from the right-most panel of Fig. 5(a). In other cases, for example, in the cases of compound angles being 30° and 60°, the effective pitches cannot be simply defined as the effusion cooling holes after rotation are not perfect aligned with

https://doi.org/10.1017/aer.2024.108 Published online by Cambridge University Press

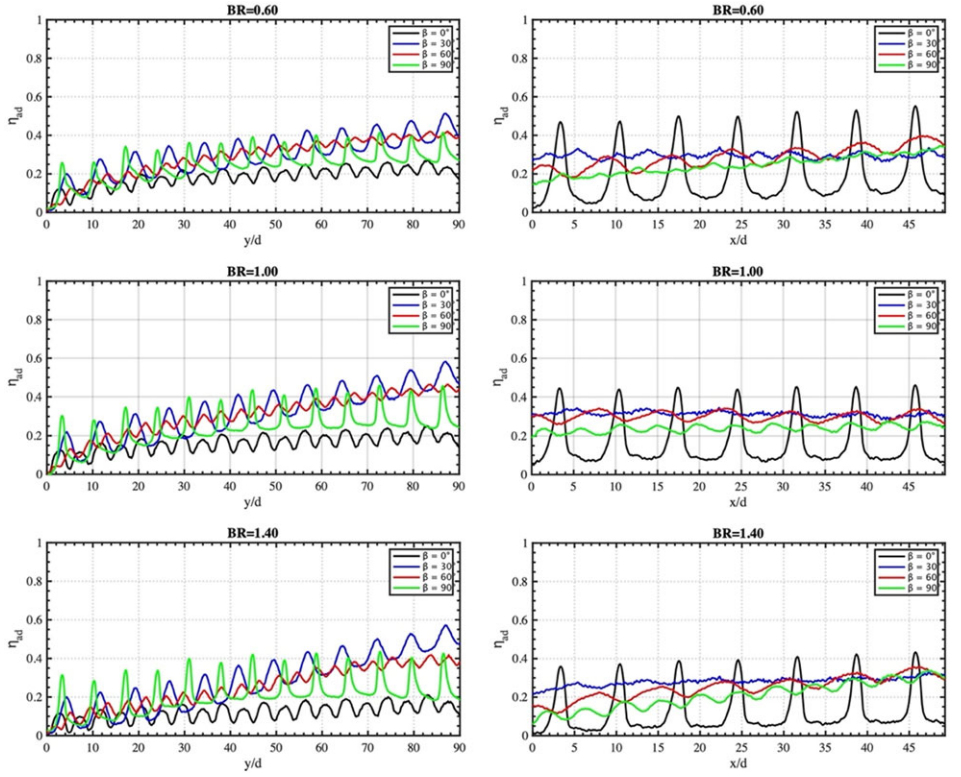

Figure 10. *Comparisons of spanwise averaged AFE (left) and streamwise averaged AFE (right) of the 2D AFE maps shown in Fig. 9.*

the main flow direction. To the knowledge of the authors, the alteration to effective cooling hole pitch due to swirling main flow has not been studied before.

Comparing to the co-linear case as the design point of effusion cooling, the combined effects of changing compound angle and pitch enhance film cooling effectiveness at all three BRs studied in this work. In the co-linear case, effusion cooling jets do not penetrate to the lateral gaps between cooling hole columns, leaving large gaps between adject cooling hole columns largely unprotected. The only mechanism for effusion cooling gas to spread out to cover inter-column gaps is mixing, which is a less efficient and less ideal way to produce cooling film as coolant being diluted and dissipated away by the main flow. The ideal method for generating cooling film is for cooling jets to penetrate spanwise while minimising the mixing between main flow and miniature effusion cooling jets. It is evident that non-zero compound angles make it easier for cooling jet to penetrate into gaps between adjacent cooling hole columns, making effusion cooling more efficient.

More quantitative analyses of 2D AFE distributions are made by comparing row-wise and column-wise mean AFE. The left panels of Fig. 10 are comparisons of row-wise AFE averages at all three BRs while the right panels are column-wise means. It is evident that a swirling main flow enhances AFE with its enhancement peaks between 30° and 60° for all BRs studied. This is good news for practical engines that set effusion cooling holes in the direction of the combustor axis. For a typical swirling number of 0.7 and a typical combustor height, the swirling main flow induces an effective compound angle of 45° [16], falling right between the ideal compound angles found in Fig.10 for all BRs. The overall mean AFE values for the entire measurement area shown in Fig. 9 that are summarised in Table 1 clearly confirm the above observation from Fig. 10. The overall mean AFE values summarised in Table 1 reveal that substantial enhancements to overall cooling film effectiveness between 27% to 135% compared to the

https://doi.org/10.1017/aer.2024.108 Published online by Cambridge University Press

Table 1. *The mean and standard deviation of the adiabatic film cooling effectiveness (η_{ad}) of the 2D AFE maps shown in Fig. 9*

	$\eta_{ad,\,mean}$			σ		
Compound angle (β)	BR = 0.6	BR = 1	BR = 1.4	BR = 0.6	BR = 1	BR = 1.4
0° (baseline)	0.2047	0.1608	0.1430	0.0801	0.0591	0.0540
30°	0.3422	0.3189	0.3373	0.1626	0.1632	0.1831
60°	0.3257	0.3027	0.2898	0.1902	0.1483	0.1439
90°	0.2619	0.2390	0.2273	0.1240	0.1130	0.1136

co-linear case ($\beta = 0°$) can be achieved by introducing main flow at 30°, 60°, and 90° to effusion cooling jets. The enhancement is more pronounced at high BRs.

It is worth a quick discussion of the role that BR plays in affect AFE at various compound angles. Effusion cooling jets lift-off and reattach back to the surface to form a cooling film, while mixing with the main flow during this process. When effusion cooling jets are co-linear with the main flow, more pronounced lift-off of cooling jets at higher BRs does not allow the coolant to effectively reattach back to and cool the plate until further downstream [25]. At the same time, enhanced jet mixing between effusion cooling jets and main flow further diminishes the AFE as BR increases. The trend that a higher BR results in less-ideal AFE when $\beta = 0°$ is evident in Fig. 10.

However, the role that BR plays at a non-zero compound angle can be more complicated as effusion jets can have a different spanwise penetration depth into the gap between effusion cooling hole columns besides the varied lift-off height as BR changes. A large spanwise penetration depth leads to a broader lateral distribution of coolant. For instance, the $\beta = 30°$ case shown in Fig. 10 reveals this complication. As BR increases from 0.6 to 1.0, as the row-wise AFE mean comparison (the blue curves in top-left panel vs. mid-left panel) indicates, the AFE enhances. This could be explained by the increased spanwise penetration depth of effusion jets into the gaps between effusion cooling column, as can be seen from the corresponding AFE 2D maps in Fig. 9. As BR further increases to 1.4 from 1.0 (the blue curves in mid-left panel vs. lower-left panel), the AFE recedes. This reduction in AFE while more coolant is being used at an increased BR can be attributed to the fact that the benefits of increased spanwise penetration at a higher BR is outweighed by the drawbacks of enhanced jet mixing between effusion cooling jets and main flow at a higher BR, which dilutes coolant substantially. The increased spanwise penetration depth of effusion jets is evident by observing the effusion jets leaving the first two row of cooling holes of three $\beta = 0°$ panels in Fig. 9 as BR increases from 0.6 to 1.4.

It should be pointed out that the AFE enhancement observed in Figs. 9 and 10 is the combined effects of simultaneously varied compound angle and pitch. As discussed earlier, although the combined effects are of practical importance to engine combustors subjecting to swirling main flow, the contributions from each factor need to be isolated and evaluated separately to better guide future effusion cooling designs since effusion cooling performance can be sensitive to cooling hole pitch [7, 26].

Revisiting Fig. 9, it may be suggested that the most efficient effusion jet spanwise penetration depth can vary depending on the effective pitch of effusion cooling holes. For example, examining the right-most panels in Fig. 9 with $\beta = 90°$, the effusion jets can penetrate deeper towards the adjacent effusion cooling hole column comparing to smaller compound angles, however, the span-wise separation between effusion cooling hole columns is reduced with the effusion cooling test coupon installed at a 90° rotation relative to the main flow. Cooling film development cannot take full advantage of the increased jet spanwise penetration depth due to the reduced separation between effusion cooling hole columns, as effusion jets clearly overshot for all BRs when $\beta = 90°$ in Fig. 9. It should be pointed out that the jet spanwise penetration increases at larger compound angles at the price of enhanced jet mixing between effusion jets and the main flow. When the jet spanwise penetration depth benefits are not fully utilised, overall AFE suffers from the enhanced jet mixing. Therefore, the optimisation of effusion cooling should be done by concurrently considering compound angle and the corresponding effective pitch.

https://doi.org/10.1017/aer.2024.108 Published online by Cambridge University Press

4.3 Sole effects of non-zero compound angles on AFE at a fixed pitch

From the discussions in Section 4.2, it is clear that the individual contributions to the combined effects of swirling main flow on AFE from a non-zero compound angle and a varied pitch need to be evaluated separately. As discussed in Section 3, effusion cooling configurations presented in Fig. 5(b) were additionally designed and fabricated for studying the sole effects of non-zero compound angles by fixing the effusion cooling hole pitch.

Figure 11 presents 2D AFE distributions for effusion cooling configurations shown in Fig. 5(b) at three BRs, 0.6, 1.0 and 1.4. Specifically, these effusion cooling configurations have the compound angles of 30°, 60° and 90° and a fixed staggered effusion cooling hole pitch ($\delta_x = 7d$ and $\delta_y = 9d$). An identical color legend is used here as that in Fig. 9, therefore direct comparisons can be made between corresponding test conditions. To avoid repetency, the 2D AFE maps of the baseline case ($\beta = 0°$) shown as the left-most panels of Fig. 9 are not reproduced here. However, the comparison can be made by referring to Fig. 9. A quick comparison with all the cases in Fig. 9, it becomes apparent that without the effects of varying pitch, non-zero compound angle alone can greatly improve AFE comparing to the co-linear case.

The effects of compound angle alone can be discerned without the complication of varying pitch. At a lower BR of 0.6, the spanwise effusion jet penetration deepens as the compound angle increases from 30° to 90°. At a 30° compound angle, the effusion jets have a span-wise penetration of roughly half of the spanwise pitch. The penetration rises to 3/4 of the spanwise pitch when the compound angle is increased to 60°. This increase of jet penetration depth is approximately proportional to the ratio of spanwise effusion jet velocity component between two compound angles of 30° and 60° for a given BR. A detailed examination of the top panels of Fig. 9 reveals that the effusion jets are more diluted at a 60° compound angle comparing to the 30° configuration due to jet mixing, despite a more significant jet penetration depth. Therefore, the sole effect of compound angle is a trade-off between jet mixing and jet penetration. Row-wise and column-wise means of AFE for the 2D AFE maps of Fig. 11 are computed, similar to those shown in Fig. 10, and are summarised in Fig. 12. Observing the top right panel of Fig. 12, which compares the column-wise means of AFE of the low BR case, it is confirmed that the 60° compound angle configuration has deeper penetration than the 30° case, as indicated by the higher trough values of the red curve as well as broader peak features; at the same time, the worsen coolant dilution due to jet mixing at the 60° compound angle configuration is evident by the lower peak value of the red curve comparing to the blue curve.

The row-wise AFE average comparisons with the BR at 0.6 show that the overall performance of two compound angles, 30° and 60°, are nearly identical over the entire streamwise span (red and blue curves in the top-left panel of Fig. 12). This indicates that the two competing effects of a non-zero compound angle, jet mixing and jet penetration, are balanced.

As the compound angle is further increased to 90° at BR = 0.6, the effusion jets quickly disappear due to intense jet mixing, as seen from the top-right panel of Fig. 11. Since the effusion jets are shortened due to jet mixing, a more considerable jet penetration depth as a potential benefit of a larger compound angle cannot be realised. The top two panels of Fig. 12 provide quantitative confirmation of the above observations. The column-wise average shown in the right panel shows that a 90° compound angle does not substantially increase jet penetration depth compared to a smaller 60° compound angle case, by comparing the widths of the peaks of the green and red curves. However, the 90° compound angle case suffers from strong jet mixing as indicated by overall lower AFE. The reduction in effusion cooling effectiveness of the 90° compound angle configuration is clearly shown in the row-wise AFE mean plots (the top left panel of Fig. 12). The comparisons of these non-zero compound angle cases clearly reveal the role that compound angle plays in effusion cooling. An ideal compound angle reaches an optimal compromise of jet penetration and jet mixing.

By examining Fig. 12 in detail, it is interesting to find that BR has a negligible effect on AFE when a non-zero compound angle is used with a fixed effusion cooling hole pitch. This surprising observation may be attributed to the fact that the pitch being fixed. When the compound angle and pitch are concurrently varied as the case investigated in Section 4.2, larger penetration depths resulting from larger

https://doi.org/10.1017/aer.2024.108 Published online by Cambridge University Press

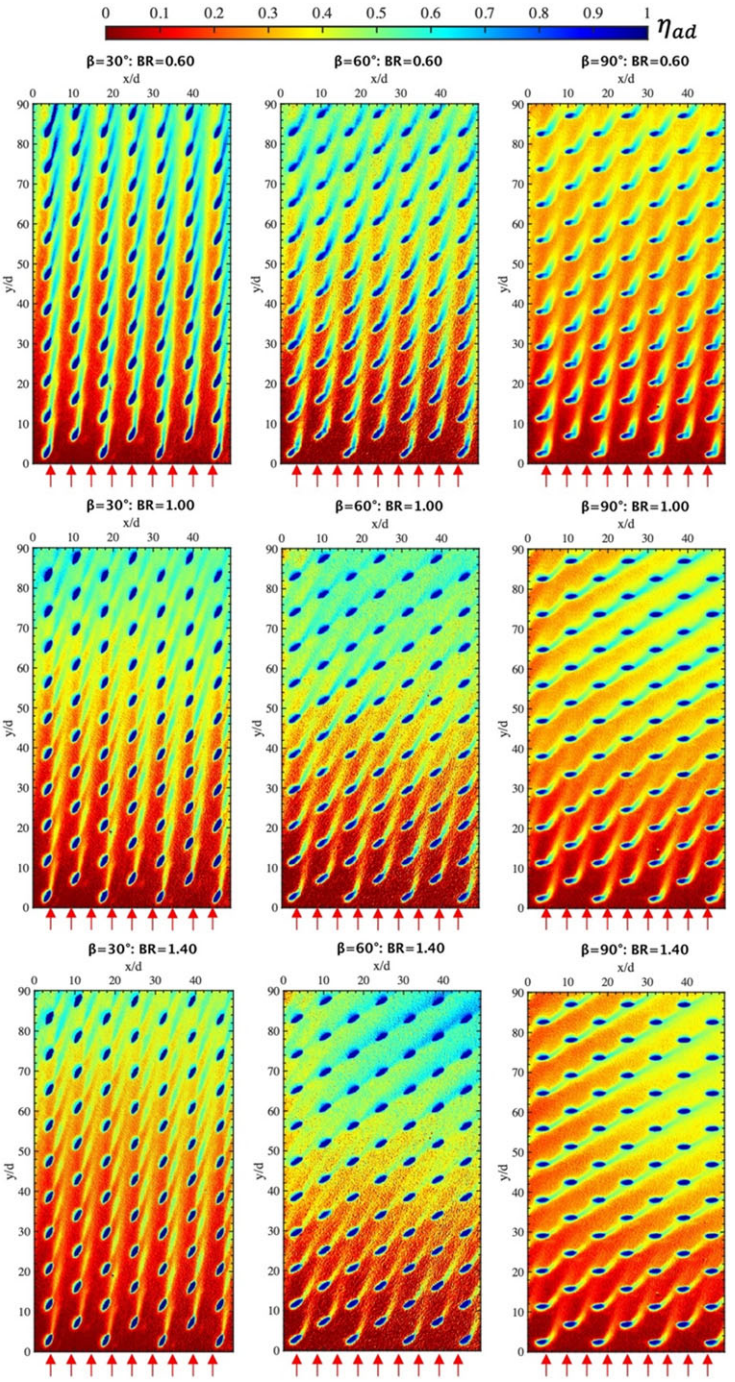

Figure 11. *Comparisons of 2D AFE distributions as a results of varying compound angles ($\beta = 30°$, 60°, and 90°), corresponding to the effusion cooling configurations presented in Fig. 5(b). As indicated in Fig. 5(b), a fixed staggered effusion cooling hole pitch ($\delta_x = 7d$ and $\delta_y = 9d$) was adopted. Red arrows indicate the main flow direction.*

https://doi.org/10.1017/aer.2024.108 Published online by Cambridge University Press

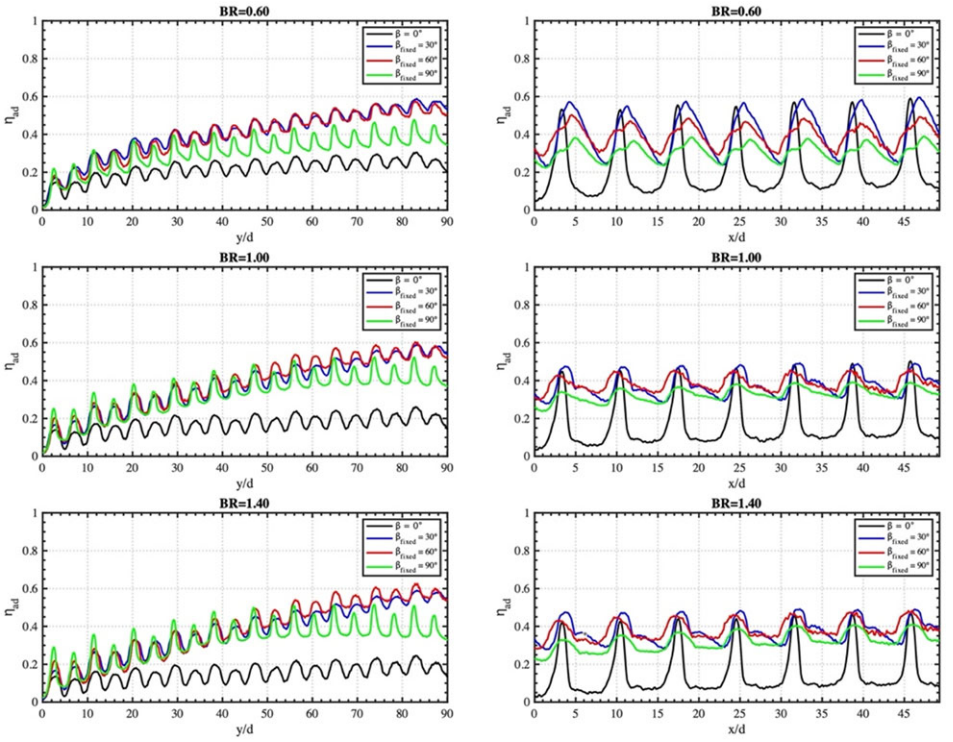

Figure 12. *Comparisons of spanwise averaged AFE (left) and streamwise averaged AFE (right) of the 2D AFE maps shown in Fig. 11 together with the baseline case shown in the left panels of Fig. 9.*

BRs are not fully capitalised due to reduced spanwise pitch when the effusion cooling coupon is rotated. In other words, with reduced spanwise pitch, larger BRs are detrimental to AFE as the effusion jets are penalised for stronger jet mixing but do not benefit from larger jet penetration. With a fixed span-wise pitch, the benefits of larger BRs can be better realised. The invariant of AFE at various BRs when a fixed pitch is used implies two conditions: 1) the span-wise pitch is large enough to take full advantages of larger jet penetration depths at higher BRs, and 2) the disadvantages of stronger jet mixing at larger BRs can be approximately offset by the benefits of larger jet penetrations. It appears that for BRs reasonably close to unity, both conditions can be met. The balance between jet mixing and jet penetration can be seen from the three right panels of Fig. 12. As the BR progressively increases from 0.6 to 1.4, all non-zero compound cases see the diminishing of AFE peak amplitudes and the broadening of the peaks.

So far, we improved the understanding of the role that a non-zero compound angle plays in the directional effects of effusion cooling. It is also discussed qualitatively in Sections 4.2 and 4.3 the role that a varied pitch might play in the directional effects of effusion cooling under swirling main flow conditions. Comparisons of AFE values between effusion cooling configurations with fixed and varied pitches at comparable compound angles may reveal pitch effects on AFE quantitatively. Figure 13 compares spanwise and streamwise AFE averages for each compound angle at a representative BR of 1, the comparisons for other BRs are not reported in this paper for simplicity as the same tendency is noted for BR 0.6 and 1.4.

Figure 13 unequivocally reveals that pitch variations induced by a swirling main flow are not beneficial to cooling film effectiveness (AFE). At compound angle of 30°, the fixed pitch has an overall AFE 20% higher than that in the varying pitch scenario by referring to the overall mean AFE values listed in Tables 1 and 2. In the case of 60°compound angle, the enhancement of AFE almost reaches 30%.

https://doi.org/10.1017/aer.2024.108 Published online by Cambridge University Press

Table 2. *The mean and standard deviation of the adiabatic film cooling effectiveness (η_{ad}) of the 2D AFE maps shown in Fig. 11*

	$\eta_{ad,\,mean}$			σ		
Compound angle (β)	BR = 0.6	BR = 1	BR = 1.4	BR = 0.6	BR = 1	BR = 1.4
0° (baseline)	0.2047	0.1608	0.1430	0.0801	0.0591	0.0540
30°	0.4133	0.3852	0.3810	0.2012	0.1781	0.1750
60°	0.4016	0.3953	0.3951	0.1945	0.1871	0.1939
90°	0.2974	0.3132	0.3024	0.1305	0.1315	0.1242

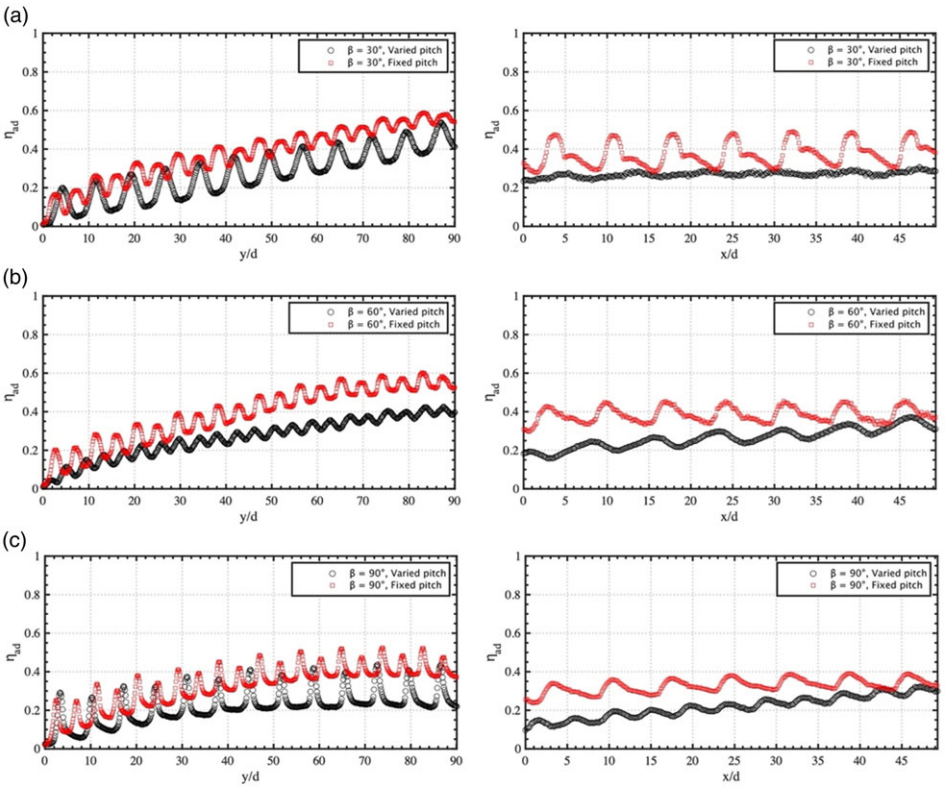

Figure 13. *The comparisons of spanwise (left) and streamwise (right) averaged AFEs between varied pitch and fixed pitch effusion cooling configurations as shown in Fig. 5 at three non-zero compound angles, (a) 30°, (b) 60° and (c) 90°. A representative BR of 1 is used for these comparisons.*

This revelation is not surprising based on the previous discussions, as all the benefits of a non-zero compound angle can be fully realised as long as the effusion jets do not overreach to the next column of effusion cooling holes. A consideration in determining optimal effusion cooling hole pitch under swirling main flow conditions may have to include the fact that some of cooling jets may become overlapping under certain pitches, the BR = 1 and $\beta = 90°$ case in Fig. 11. Overlapping effusion cooling jets is apparently less-ideal for producing a uniform cooling film, which could the subject of a future study specifically on pitch optimisation under swirling main flow conditions.

To guide the optimisation of compound angle when the fixed pitch shown in Fig. 5(b) is used, Fig. 14 is compiled based on the 2D AFE maps presented in Fig. 11. For each BR and compound angle combination, a 2D AFE map in Fig. 11 is equally divided along the flow direction into 10 sub-regions and

https://doi.org/10.1017/aer.2024.108 Published online by Cambridge University Press

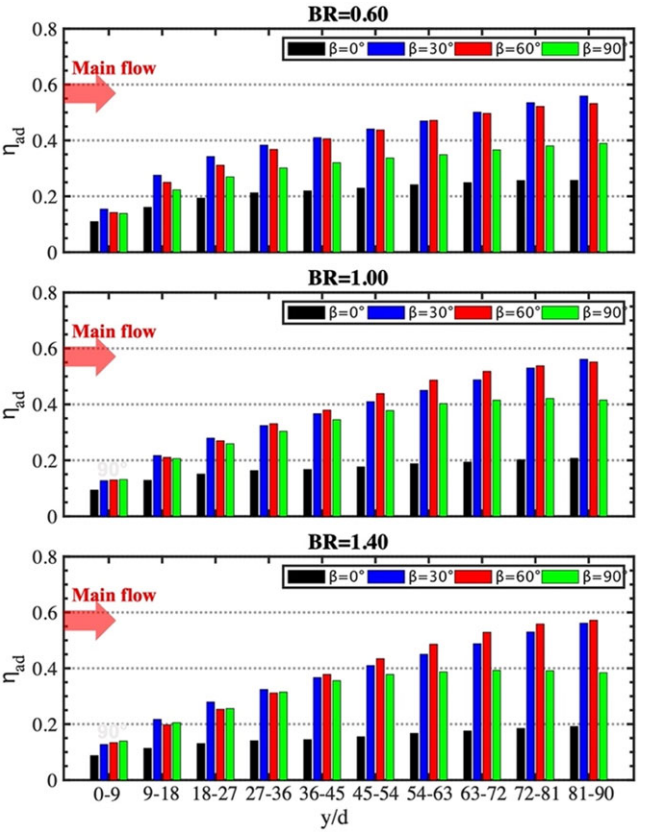

Figure 14. *Mean AFE for 10 equal blocks along the mean flow direction for each 2D AFE map shown in Fig. 11.*

a mean AFE value is computed for each sub-region. By plotting the mean AFEs for each sub-region along the main flow direction as histograms, the optimal compound angles for the prescribed fixed pitch can be determined. Three observations can be made for the fixed pitch configuration investigated in this study from Fig. 14: 1) two compound angles, 30° and 60°, appear to be optimal for enhancing AFE, 2) regardless of BR, the optimal compound angle remains the same, and 3) regardless the cooling film development stage along the main flow direction, the optimal compound angle remains the same. These observations indicate that for the fixed pitch studied here, the choice of optimal compound angle is simple and universal: a compound angle between 30° and 60°.

4.4 Other discussions

It should be pointed out that the experiments of this study were conducted with the coolant to mainstream density ratio near unity (DR ≈ 1) while for engine conditions the typical value is DR ≈ 2. Higher AFE values can be achieved under engine conditions with higher density ratios, because higher density ratios lead to lower coolant velocity at fixed BRs. Consequently, the results presented in this study is a conservative representation of AFE performance under engine conditions. However, the difference in AFE due to variations in DR is expected to be small, with the difference in AFE less than 20% for coolant DR ≈ 2 compared to DR ≈ 1.2 in the vicinity to the effusion hole but was essentially zero farther downstream [27–29].

https://doi.org/10.1017/aer.2024.108 Published online by Cambridge University Press

In addition, the turbulence level of the experiments performed in this study is estimated to be 3%. The turbulence level of a gas turbine combustor was previously measured to be 6% and 9% at non-reacting and combustion conditions, respectively, along the combustor centreline [30]. The impact of turbulence intensity on cooling film effectiveness has been well-established [31, 32]: at the optimal momentum flux ratio, a high turbulence level of Tu = 17% caused a factor of two decrease in film effectiveness near the effusion hole comparing to a low turbulence level flow (Tu = 0.3%), and almost a complete loss of cooling for x/d > 25 [32].

However, it should be pointed out that the combustor investigated by the previous study have strong impinging jets in crossflow in the forms of dilution air jets. It has been established that a primary source of turbulence in a gas turbine combustor is impinging jets in crossflow [33]. Other than rich-burn/quick–mix/lean-burn (RQL) combustor, modern gas turbine combustors have largely moved away from large impinging dilution air jets, therefore, a reduced turbulence level in combustors could be expected. In addition, the earlier study also found that the difference in cooling film effectiveness between two main flows of higher turbulence levels (Tu = 10% vs. Tu = 17%) is insignificant. Therefore, we believe the findings of this study is valid for realistic engine conditions. Nevertheless, a future study is warranted to confirm that the proposed optimal compound angle is also valid for modestly high turbulence levels (6-9%).

5.0 Conclusions

Typically, gas turbine combustors featuring effusion cooling have the effusion cooling holes aligned with the axis of the combustor. However, the main flow in gas turbine combustors swirls for flame stabilisation, which induced a non-zero compound angle between main flow and effusion cooling jets. The swirling main flow also alters the effective pitch of effusion cooling holes. The directional effects of effusion cooling induced by a swirling main flow are the results of a non-zero compound angle and a varied pitch simultaneously acting on effusion jets. Surprisingly, these important directional effects induced by a swirling main flow received little attention in the literature.

Two sets of experiments were designed. The first set of experiment mimics the scenario that a piece of effusion cooled engine combustor liner subjects to various swirling levels of main flow, rendering four discrete compound angles: 0°, 30°, 60° and 90°. The pitch of effusion cooling holes is defined when the compound angle β is 0° (co-linear baseline case) as $\delta_x = 7d$ and $\delta_y = 9d$, staggered. The same effusion cooling test coupon was rotated to achieve three non-zero compound angles: 30°, 60° and 90°. Due to the rotation of test coupon, the effective pitch of the effusion cooling plate is concurrently varied with compound angle. It is confirmed that non-zero compound angles make it easier for cooling jet to penetrate into gaps between adjacent cooling hole columns, making effusion cooling more efficient. Substantial enhancements to overall cooling film effectiveness between 27% to 135% was observed compared to the co-linear baseline case ($\beta = 0°$) by introducing the main flow at 30°, 60°, and 90° to effusion cooling jets; the AFE enhancement peaks between 30° and 60° for all BRs studied. In addition, the AFE enhancement due to swirling main flow is more pronounced at high BRs.

Although the first set of experiments is more relevant to engine realties, the combined effects of non-zero compound angle and varied pitch on AFE makes it difficult to determine the contributions from each factor separately. The second set of experiments were performed with a fixed pitch ($\delta_x = 7d$ and $\delta_y = 9d$, staggered) that doesn't vary with compound angle. Three additional effusion cooling coupons were fabricated to achieve three non-zero compound angles: 30°, 60° and 90°. Without the complication of varying pitch, the effects of compound angle alone can be clearly discerned: a non-zero compound angle leads to a trade-off between jet mixing and jet penetration. Larger jet penetration depths usually can result from larger compound angles, promoting the spreading of coolant into the gaps between adjacent effusion cooling hole columns and enhancing AFE. However, the competing effect of adopting larger compound angles is that stronger jet mixing can occur, resulting in excessive losses of coolant to the main flow, diminishing AFE.

https://doi.org/10.1017/aer.2024.108 Published online by Cambridge University Press

When the effects of varying pitch are excluded, a good balance of jet penetration and jet mixing can be achieved for two moderate compound angles, 30° and 60°, regardless of BR or the cooling film development stage. Therefore, the choice of optimal compound angle is simple and universal: a compound angle between 30° and 60°. The invariant of AFE at various BRs when a fixed pitch is used implies two conditions: 1) the span-wise pitch is large enough to take full advantages of larger jet penetration depths at higher BRs, and 2) the disadvantages of stronger jet mixing at larger BRs can be approximately offset by the benefits of larger jet penetrations. We propose a 45° compound angle as the starting point for future effusion cooling design optimisations.

It is hypothesised that a varying pitch affects AFE by potentially limiting the benefits of larger jet penetration depths resulting from larger compound angles. When the effusion cooling coupon is rotated and the spanwise pitch is reduced, the effusion jets resulting from larger compound angles not only fully penetrates the gap between adjacent effusion cooling hole columns, but also overshoot. When effusion jets overshoot the reduced spanwise pitch, the effusion jets are penalised for coolant losses due to stronger jet mixing but do not benefit from larger jet penetration. The similar reduction in AFE at higher BRs can be observed when the spanwise pitch is reduced, because at larger BRs the effusion jets are again penalised for stronger jet mixing but do not benefit from larger jet penetration. With a fixed span-wise pitch that can take full advantage of increased jet penetration depth, the benefits of a larger BR or a larger compound angle up to 60° can be better realised.

With the optimal compound angle proposedly set at 45°, the next step is to search for an optimal pitch. As discussed earlier, one factor may have to be considered in determining optimal effusion cooling hole pitch is that some of effusion jets may overlap at certain BR. Overlapping effusion cooling jets is apparently less-ideal and inefficient for producing a uniform cooling film. This factor may be investigated in the future when pitch optimisation is studied.

Finally, in future effusion cooling design optimisations, the swirling effect of the main flow has to be taken into account. The optimal compound angle of 45° that we proposed here should be achieved considering the combustor swirl number. In addition, it is the effective pitch, resulting from the nominal pitch and swirling main flow, that should be optimised, instead of the nominal one.

Acknowledgments. The work is supported by the National Research Council of Canada (NRC)'s National Program Office under the Ideation New Beginnings Program (No. 577) and Postdoctoral Fellowship Program (PDF2021-06). Additional funding for the work is provided by the NRC's Aerospace Research Center under the LEAP Program (LEAP-012). The authors would like to thank NRC Technical Officers Mart Jonathan Regalado & Yin Yang for their technical support.

References

[1] S. Ahmed, P. Singh, and S.V. Ekkad, "Comparison of Different Combustion Liner Cooling Techniques under Non-Reacting Conditions for a Lean Pre-Mixed Fuel Nozzle," *AIAA Scitech 2019 Forum*, pp. 1–13, 2019.

[2] D.G. Ritchie, A.J. Click, P.M. Ligrani, F. Liberatore, R. Patel, and Y.H. Ho, "Double Wall Cooling of an Effusion Plate with Cross Flow and Impingement Jet Combination Internal Cooling: Comparisons of Main Flow Contraction Ratio Effects," *AIAA Propulsion and Energy 2019 Forum*, pp. 1–18, 2019.

[3] P.W. Schilke, "Advanced Gas Turbine Materials and Coatings," *Report GER-3569G, GE Energy*, Schenectady, NY, 2004.

[4] B. Goswami, S.K. Sahay, and A.K. Ray, "Application of Thermal Barrier Coatings on Combustion Chamber Liners – A Review," *High Temperature Materials and Processes*, vol. **23**, no. 3, pp. 211–236, 2004.

[5] P. Grootenhuis, "The Mechanism and Application of Effusion Cooling∗," *The Journal of the Royal Aeronautical Society*, vol. **63**, no. 578, pp. 73–89, 1959.

[6] K.M.B. Gustafsson, "Experimental Studies of Effusion Cooling," Ph. D. Dissertation, Department of Thermo and Fluid Dynamics, Charlmers University of Technology, Göteborg, Sweden, 2001.

[7] H.H. Cho, D.H. Rhee, and R.J. Goldstein, "Effects of Hole Arrangements on Local Heat/Mass Transfer for Impingement/Effusion Cooling with Small Hole Spacing," *Journal of Turbomachinery*, vol. **130**, no. 4, 2008.

[8] R. Krewinkle, "A Review of Gas Turbine Effusion Cooling Studies," *International Journal of Heat and Mass Transfer*, vol. **66**, pp. 706–722, 2013.

[9] G. Cerri, A. Giovannelli, L. Battisti, and R. Fedrizzi, "Advances in Effusive Cooling Techniques of Gas Turbines," *Applied Thermal Engineering*, vol. **27**, no. 4, pp. 692–698, 2007.

[10] D.G. Bogard, "Gas Turbine Film Cooling," *Journal of Propulsion and Power*, vol. **22**, no. 2, pp. 249–270, 2006.

[11] B. SEN, D.L. Schmidt and D.G. Bogard, "Film Cooling with Compound Angle Holes: Heat Transfer," *Journal of Turbomachinery*, vol. 118, no. 4, pp. 800-806, 1996.

https://doi.org/10.1017/aer.2024.108 Published online by Cambridge University Press

[12] L.C Paitich, P. Richer, B. Jodoin, Y. Pyo, S. Yun, and Z. Hong, "Directional Effects of Effusion Cooling on the Cooling Film Effectiveness," *AIAA Journal*, pp.1–12, 2021.
[13] T. Liu, B.T. Campbell, S.P. Burns, and J.P. Sullivan, "Temperature- and Pressure-Sensitive Luminescent Paints in Aerodynamics," *Applied Mechanics Reviews*, vol. **50**, no. 4, pp. 227–246, 1997.
[14] J.W. Gregory, K. Asai, M. Kameda, T. Liu, and J.P. Sullivan, "A review of pressure-sensitive paint for high-speed and unsteady aerodynamics," *Proceeding of the Institution of Mechanical Engineers, Part G: Journal of Aerospace Engineering*, vol. 222, no. 2, pp. 249–290, 2008.
[15] A. Andreini, B. Facchini, A. Picchi, L. Tarchi, and F. Turrini, "Experimental and Theoretical Investigation of Thermal Effectiveness in Multi-Perforated Plates for Combustor Liner Effusion Cooling," *Journal of Turbomachinery*, vol. **136**, no. 9, pp. 1–13, 2014.
[16] Y. Pyo, M. Broumand, J. Son, P. Richer, B. Jodoin and Z. Hong, "Enhanced Adiabatic Film Cooling Effectiveness by Varying Compound Angle," *Proceedings of the ASME Turbo Expo2024*, 2024.
[17] L. Andrei, A. Andreini, C. Bianchini, G. Caciolli, B. Facchini, A. Picchi, L. Tarchi, and F. Turrini, "Effusion cooling plates for combustor liners: experimental and numerical investigations on the effect of density ratio," *Energy Procedia*, no. 45, pp. 1402–1411, 2014.
[18] G. Barigozzi, C. Mucignat, H. Abdeh, D. Scandella and G. Dolci, "Assessment of binary PSP technique for film cooling effectiveness measurement on nozzle vane cascade with cutback trailing edge," *Experimental Thermal and Fluid*, vol. **97**, no. 201, pp. 431–443, 2014.
[19] Innovative Scientific Solutions Inc. Binary Pressure-Sensitive Paint (http://www.psp-tsp.com). Accessed 20 April 2023.
[20] D. McLean, "Referenced pressure paint and the ratio of ratios," *Proceedings of the Sixth Annual Pressure Sensitive Paint Workshop*, The Boeing Company, Seattle, Washington, pp. 11–1:35, 1998
[21] T. Liu, T. Ben and J.P. Sullivan," Pressure Sensitive Paints," *NASA Review Article*, 2000
[22] T.V. Jones," Theory for the Use of Foreign Gas in Simulating Film Cooling," *International Heat and Fluid Flow*, vol. 20, no. 3, pp. 349–354, 1999
[23] J.C. Han and A.P. Rallabandi, "Turbine Blade Film Cooling Using PSP Technique," *Front. Heat Mass Transfer*, vol. **1**, no. 1, p. 013001, 2010
[24] Z. Lei, A. Mahallati, M. Cunningham, and P. Germain, "Influence of Inlet Swirl on the Aerodynamics of a Model Turbofan Lobed Mixer," *ASME International Mechanical Engineering Congress and Exposition*, pp. 807–819, 2010.
[25] J.J. Scrittore, K.A. Thole and S.W. Burd, "Investigation of Velocity Profiles for Effusion Cooling of a Combustor Liner," *Journal of Turbomachinery*, vol. **129**, pp. 518–526, 2007.
[26] A.M.A. Dabagh, G.E. Andrews, R.A.A. Abdul Husain, C.I. Husain, A. Nazari and J. Wu, "Impingement/Effusion Cooling: The Influence of the Number of Impingement Holes and Pressure Loss on the Heat Transfer Coefficient," *Journal of Turbomachinery*, vol. **112**, no. 3, pp. 367–476, 1990.
[27] S. Baldauf, M. Scheurlen, A. Schulz and S. Witting, "Correlation of Film-Cooling Effectiveness from Thermographic Measurements at Enginelike Conditions," *Journal of Turbomachinery*, vol. **124**, pp. 686–698, 2002.
[28] A.K. Sinha, D.G. Bogard and M.E. Crawford, "Film Cooling Effectiveness Downstream of a Single Row of Holes with Variable Density Ratio," *Journal of Turbomachinery*, vol. **113**, no. 3, pp. 442–449, 1991.
[29] D.R. Pedersen, E. Eckert and R. Goldstein, "Film Cooling with Large Density Differences Between the Mainstream and the Secondary Fluid Measured by the Heat-Mass Transfer Analogy," *ASME Journal of Heat Transfer*, vol. **99**, pp. 620–627, 1977.
[30] C.J. Marek, "Combustor Turbulence," Transition in Turbines, NASA Conference Publication, 2386.
[31] X. Chen, J. Krawciw, H. Xia, P.A. Denman, C. Bonham and J.F. Carrotte, "Study of an effusion-cooled plate with high level of upstream fluctuation," *Applied Thermal Engineering*, vol. **184**, 2021.
[32] D.L. Schmidt and D.G. Bogard, "Effects of Free-Stream Turbulence and Surface Roughness on Film Cooling," ASME Paper 96-GT-462, 1996.
[33] M. Folk, R.J. Miller and J.D. Coull, "The Impact of Combustor Turbulence on Turbine Loss Mechanisms," *Journal of Turbomachinery*, vol. **142**, no. 9, 091009, 2020.

Cite this article: Pyo Y., Son J., Richer P., Jodoin B., Broumand M., Yun S. and Hong Z. (2025). Isolating influences of varying pitch from the effects of non-zero compound angles on effusion cooling. *The Aeronautical Journal*, **129**, 63–83. https://doi.org/10.1017/aer.2024.108